

A new superconductor derived from topological insulator heterostructure

Satoshi Sasaki,¹ Kouji Segawa,¹ and Yoichi Ando^{1,*}

¹*Institute of Scientific and Industrial Research, Osaka University, Ibaraki, Osaka 567-0047, Japan*
(Dated: June 21, 2021)

Topological superconductors (TSCs) are of significant current interest because they offer promising platforms for finding Majorana fermions. Here we report a new superconductor synthesized by intercalating Cu into a naturally-formed topological insulator (TI) heterostructure consisting of Bi_2Se_3 TI units separated by nontopological PbSe units. For the first time in a TI-based superconductor, the specific-heat behavior of this material suggests the occurrence of unconventional superconductivity with gap nodes. The existence of gap nodes in a strongly spin-orbit coupled superconductor would give rise to spin-split Andreev bound states that are the hallmark of topological superconductivity. Hence, this new superconductor emerges as an intriguing candidate TSC.

PACS numbers: 74.10.+v, 74.25.Bt, 74.70.Dd, 03.65.Vf

A major theme in current condensed matter physics is to understand and explore the roles of topology in quantum mechanics. In topological insulators (TIs), a non-trivial topology of the quantum-mechanical wave functions leads to the appearance of gapless conducting states at the boundary (i.e. edge or surface) [1–3]. Topological superconductors (TSCs) are conceptually similar to TIs and are characterized by gapless quasiparticle states at the boundary [1, 4–6], but an important distinction from TIs is that the boundary state of a TSC is a good place to look for Majorana fermions [7–9], which possess a distinct property that particles are their own antiparticles and would be useful for fault-tolerant topological quantum computing. In this context, superconductors derived from TIs are of particular interest, because the strong spin-orbit coupling inherent to TIs may lead to unconventional pairing that is prerequisite to TSCs [9]. However, there have been only a few cases in which superconductivity is found in doped TIs [10–16], and it is strongly desired that a new superconductor with promising indications of unconventional superconductivity is discovered in a doped TI.

Recently, two of the authors have contributed to the discovery of an interesting new topological insulator [15], $(\text{PbSe})_5(\text{Bi}_2\text{Se}_3)_6$. This is a member of the Pb-based homologous series of compounds [18], $(\text{PbSe})_5(\text{Bi}_2\text{Se}_3)_{3m}$ ($m = 1, 2, \dots$), which naturally form multilayer heterostructures of a topological insulator (Bi_2Se_3) and an ordinary insulator (PbSe). It was found that at $m = 2$, the PbSe unit works as a block layer and the topological boundary states are encapsulated in each Bi_2Se_3 unit, making the system to possess quasi-two-dimensional (quasi-2D) states of topological origin throughout the bulk. Bi_2Se_3 consists of a stack of Se-Bi-Se-Bi-Se quintuple layers (QLs), and the $m = 2$ member of $(\text{PbSe})_5(\text{Bi}_2\text{Se}_3)_{3m}$ has 2 QLs in its Bi_2Se_3 unit [see Fig. 1(a)]. In the middle of this 2-QL unit is a van der Waals gap, into which intercalations of atoms or molecules are possible.

Motivated by the occurrence of superconductivity in

Bi_2Se_3 upon Cu intercalation [10], we tried to make $(\text{PbSe})_5(\text{Bi}_2\text{Se}_3)_6$ (hereafter called PSBS) superconducting via Cu intercalation. We adopted the electrochemical technique which we developed for making high-quality $\text{Cu}_x\text{Bi}_2\text{Se}_3$ superconductors [19], and we have succeeded in synthesizing [20] a new superconductor with this strategy. Intriguingly, this new material, $\text{Cu}_x(\text{PbSe})_5(\text{Bi}_2\text{Se}_3)_6$ (called CPSBS), turned out to be quite different from its cousin, $\text{Cu}_x\text{Bi}_2\text{Se}_3$: First, this new superconductor presents an unusual specific-heat behavior which suggests unconventional superconductivity. Second, nearly 100% superconducting samples can sometimes be synthesized, which makes it easier to elucidate its intrinsic nature.

Figure 1(b) shows the resistivity data for PSBS and CPSBS ($x = 1.36$). The Cu intercalation causes a sharp superconducting transition at 2.85 K, and at the same time, it introduces moderate electron scattering to enhance the residual resistivity. The carrier density increases from $n_e \simeq 4 \times 10^{20}$ in PSBS to $1.2 \times 10^{21} \text{ cm}^{-3}$ in CPSBS ($x = 1.36$), which suggests that each intercalated Cu introduces about 0.7 electron on average [20]. The Hall resistivity data indicate that the transport is governed by only one band (see Fig. S1(b) of the Supplemental Material [20]), suggesting that the topological and nontopological bands of the Bi_2Se_3 unit [15] may well have merged at the chemical potential of CPSBS. As shown in Figs. 1(c) and 1(d), in the present set of samples the onset of superconductivity was essentially independent of x and was always around 2.9 K for $x = 0.3 - 2.3$, whereas the shielding fraction (the fraction of the sample volume from which the magnetic field is kept out due to superconductivity after zero-field cooling) was very much sample dependent; note that, in the case of type-II superconductors, the shielding fraction is a better measure of the superconducting volume fraction than the Meissner fraction measured upon field cooling, because the latter is significantly affected by flux trapping. The random nature of the obtained shielding fraction vs x signifies the difficulty in synthesizing a homogeneous

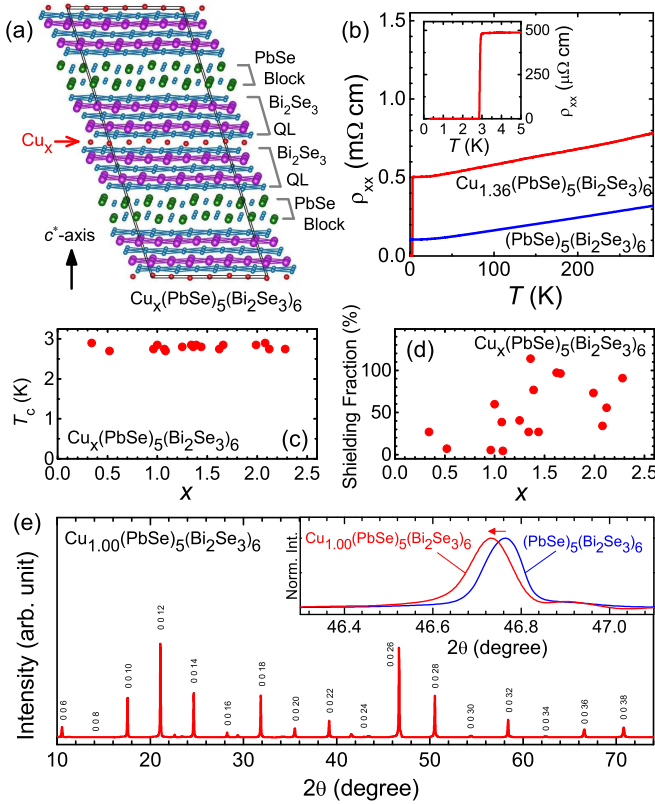


FIG. 1: (Color online) $\text{Cu}_x(\text{PbSe})_5(\text{Bi}_2\text{Se}_3)_6$ superconductor. (a) Crystal structure based on the data for PSBS [18]. Cu atoms are intercalated into the van der Waals gaps marked by red arrow. (b) Temperature dependencies of the resistivity ρ_{xx} for PSBS and CPSBS ($x = 1.36$). Inset shows the sharp superconducting transition at 2.85 K. (c) Onset T_c measured by dc magnetic susceptibility for samples with various x values. (d) Shielding fractions of the samples presented in (c) at 1.8 K. (e) XRD pattern measured on a cleaved surface (ab plane) of a superconducting CPSBS sample with $x = 1.00$ (shielding fraction $\sim 60\%$), where the peak pattern is essentially the same as that of pristine PSBS. Inset compares the positions of the prominent (0 0 26) peak for PSBS and CPSBS, which demonstrates that the periodicity perpendicular to the layers is slightly enlarged from 50.460(1) Å to 50.508(1) Å after the Cu intercalation.

superconductor with intercalation, and a majority of our samples are inhomogeneous. Nonetheless, we have been able to achieve essentially 100% shielding fraction in a few samples with $x = 1.3 - 1.7$, and in those special samples the roles of minority phases can be largely neglected. The x-ray diffraction (XRD) data from cleaved surfaces of single-crystalline CPSBS indicate that the system essentially preserves the same crystal structure of PSBS with a slightly elongated c^* -axis, as is expected for an intercalated material [Fig. 1(e)]; however, it is beyond the scope of this paper to precisely determine the crystallographic structure, including the exact position of Cu, of this obviously complicated material.

In the following, we focus on two samples with $x =$

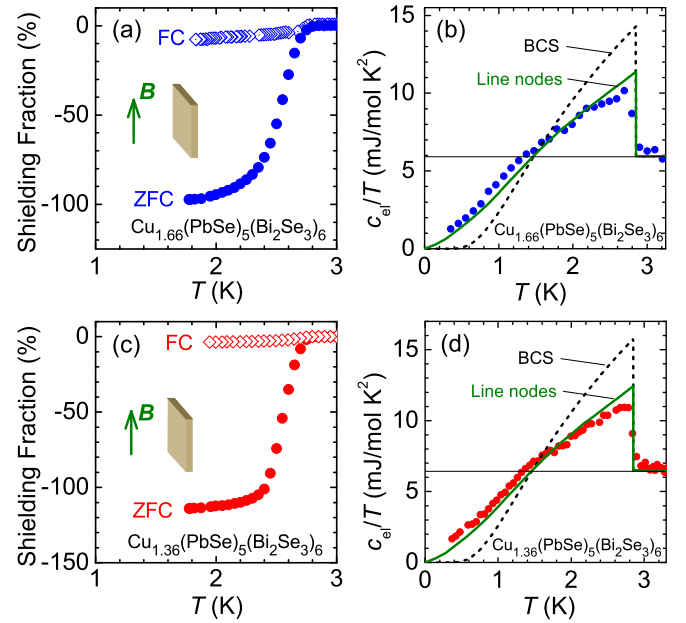


FIG. 2: (Color online) Shielding fraction and specific heat. (a) and (c) Temperature dependencies of the dc magnetic susceptibility measured in 0.2 mT applied parallel to the ab plane with the field-cooling (FC) and zero-field-cooling (ZFC) procedures for (a) $x = 1.66$ and (c) $x = 1.36$, presented in terms of the shielding fraction. Since the demagnetization effect is minimal for this geometry and the sample shape was irregular, we did not make any correction for it [the $x = 1.66$ (1.36) sample was 0.23 (0.16) mm thick and 1.6 ± 0.3 (1.7 ± 0.35) mm long along the B field]. (b) and (d) Superconducting transition in c_{el}/T in 0 T obtained after subtracting the phonon contribution determined in 2 T (see Fig. S2 [20]). The dashed line is the weak-coupling BCS behavior (coupling constant $\alpha = 1.76$) for T_c of 2.85 K. The green solid line is the theoretical curve for d -wave pairing on a simple cylindrical Fermi surface with line nodes along the axial direction [22]. Horizontal solid line corresponds to γ_N .

1.36 and 1.66, which presented essentially 100% shielding fractions as shown in Figs. 2(a) and 2(c). Figures 2(b) and 2(d) show the behavior of the electronic specific heat c_{el} in terms of c_{el}/T vs T for the two samples; those data were obtained after subtracting the phonon contribution determined in 2 T described in Fig. S2 of the Supplemental Material [20]. The two samples consistently present two unconventional features that become apparent when compared with the conventional weak-coupling BCS behavior [21] shown with dashed lines: First, the jump height at T_c is much smaller than the prediction of the BCS theory, $1.43 \gamma_N$, where γ_N is the normal-state electronic specific-heat coefficient corresponding to the horizontal solid lines. Second, c_{el}/T decreases much more slowly than the BCS behavior; in particular, c_{el}/T keeps showing a sizable temperature dependence even at our lowest temperature of 0.35 K ($T/T_c = 0.12$), whereas c_{el}/T should already become negligible at such a low

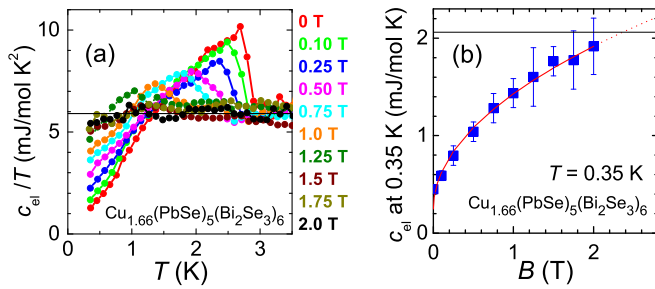


FIG. 3: (Color online) Specific heat in magnetic fields. (a) Temperature dependencies of c_{el}/T in various magnetic fields ($B \perp ab$) for $x = 1.66$. Small Schottky anomaly that becomes non-negligible above ~ 1.5 T has been subtracted (see [20]). Horizontal solid line corresponds to γ_N . (b) Magnetic-field dependence of c_{el} at 0.35 K taken from the data in (a). The red solid line is the best fit of the function $aB^n + c_0$ to the data, yielding $n = 0.50 \pm 0.06$, $a = 1.2 \pm 0.1$ ($\text{mJ mol}^{-1} \text{K}^{-1} \text{T}^{-n}$), and $c_0 = 0.25 \pm 0.09$ ($\text{mJ mol}^{-1} \text{K}^{-1}$). Horizontal solid line corresponds to $\gamma_N T$ at $T = 0.35$ K.

temperature in the BCS case. It is reassuring that those unconventional features are exactly reproduced in two different samples.

Such a peculiar behavior in c_{el}/T suggests the existence of nodes in the superconducting gap for the following reasons: First, when the gap has nodes, the averaged gap magnitude becomes smaller than the fully-gapped case, and the specific-heat jump is naturally reduced [6, 21]; the green solid line in Figs. 2(b) and 2(d) gives an example for the d -wave superconductivity with line nodes [22]. Second, in contrast to the conventional BCS case in which c_{el}/T decreases exponentially at low T because of a finite activation energy, the existence of nodes allows thermal excitations of quasiparticles down to very low temperatures, changing the T dependence of c_{el}/T from exponential to a power law [6].

As one can see in Figs. 2(b) and 2(d), our data, particularly the strong T dependence near 0 K, bear striking similarity to the theoretical c_{el}/T behavior expected for a superconductor with line nodes [22], which point to the realization of unconventional superconductivity in CPSBS. Of course, specific-heat measurements alone are not sufficient for unambiguously nailing down the existence of nodes, because a multiband superconductor with a very small gap in one of the bands or an anisotropic s -wave superconductor with very small gap minima would give rise to a c_{el}/T behavior similar to what we found in CPSBS. Hence, phase-sensitive measurements are crucially important in the future research of this material. Also, STM and NMR experiments would be very useful for elucidating the realization of unconventional superconductivity.

Note that in the case of nodal superconductors, impurity scattering causes a finite density of quasiparticle states at 0 K, causing $(c_{el}/T)_{T \rightarrow 0}$ to be finite even in a

100% superconducting sample; this may also be the case in the present system, given the relatively large residual resistivity. Also, it is prudent to mention that the spin-orbit scattering [23] is pair breaking and may mimic the c_{el}/T behavior observed here, so its role should be elucidated in future. Nevertheless, it is fair to note that in $\text{Cu}_x\text{Bi}_2\text{Se}_3$, where the spin-orbit scattering should be of similar strength, the c_{el}/T behavior was found to obey the simple BCS theory [19].

Due to the quasi-2D nature of the parent material PSBS [15], the superconductivity in CPSBS is likely to be realized on a quasi-2D Fermi surface, which is distinct from the three-dimensional (3D) bulk Fermi surface of Bi_2Se_3 . This implies that the theory of 3D topological superconductivity proposed for $\text{Cu}_x\text{Bi}_2\text{Se}_3$ [9] is not directly applicable. Nevertheless, it is still expected that strong spin-orbit coupling responsible for the topological nature of the parent material causes the effective pairing interaction to become spin dependent, which would lead to unconventional superconductivity [9]. When the Fermi surface is quasi-2D, a node in the unconventional superconducting gap is naturally extended along the c^* axis, forming a line node in the 3D Brillouin zone. It is thus expected that, if gap nodes were to be present in CPSBS, the c_{el}/T behavior should be close to that of a superconductor with line nodes.

The possible existence of line nodes in CPSBS is further supported by the magnetic-field dependence of the specific heat. Figure 3(a) shows the c_{el}/T vs T plots for various magnetic fields applied perpendicular to the ab plane described in Fig. S2 of the Supplemental Material [20], from which we extract the magnetic-field dependence of c_{el} at the lowest temperature, 0.35 K; here, to make our best effort to quantify its behavior, the data are corrected for a small Schottky anomaly [20], which is only $\lesssim 20\%$ even at the upper critical field and is comparable to the error bar. The obtained $c_{el}(B)$ behavior at 0.35 K [Fig. 3(b)] is clearly nonlinear in B . Note that in conventional BCS superconductors c_{el} increases essentially linearly with B , because the number of induced quasiparticles is proportional to the number of vortices. On the other hand, in nodal superconductors, the Doppler shift of the quasiparticle excitations (so-called Volovik effect) causes more quasiparticles to be created per vortex than in the BCS case [24]; for line nodes, Volovik showed [24] that c_{el} increases as $\sim \sqrt{B}$. Indeed, our data are best described with $c_{el} \sim B^{0.5}$, supporting the existence of line nodes.

Figures 4(a) and 4(c) show the magnetic-field-induced resistive transitions at various temperatures in $B \perp ab$ and in $B \parallel ab$, respectively, from which the resistive upper critical fields $B_{c2\perp}(T)$ and $B_{c2\parallel}(T)$ are extracted. We plot in Figs. 4(b) and 4(d) the magnetic field values at which 2%, 50%, and 98% of the normal-state resistivity ρ_N is recovered at a given temperature. It is customary to use 50% ρ_N for defining B_{c2} [13, 14, 25]. In Fig. 4(b), the on-

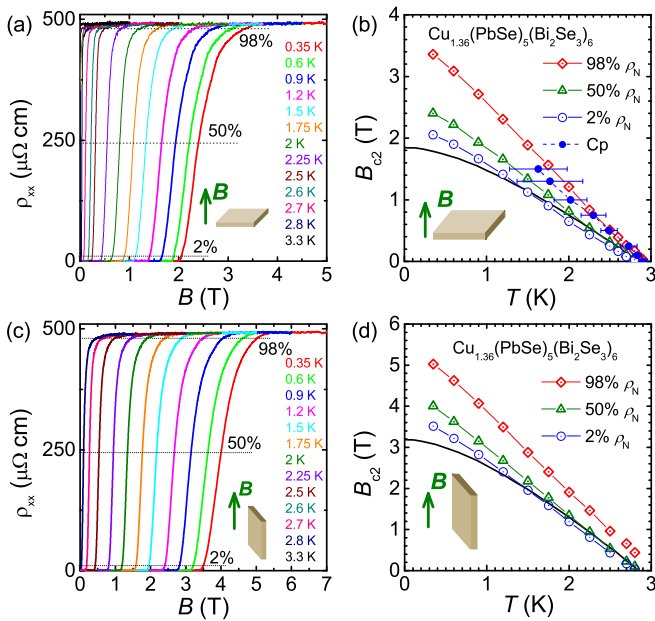


FIG. 4: (Color online) Upper critical field B_{c2} . (a) and (c) Magnetic-field-induced resistive transitions measured at various temperatures in the $x = 1.36$ sample for (a) $B \perp ab$ and (c) $B \parallel ab$. Three levels of the resistivity ρ_{xx} in those transitions, corresponding to 2%, 50%, and 98% of ρ_N (shown by dotted lines), are used for determining the depinning, mid-point, and onset fields, respectively; 50% ρ_N is the definition of B_{c2} . (b) and (d) B vs T phase diagrams obtained from the data in (a) and (c), respectively. The black solid lines are the conventional $B_{c2}(T)$ behavior given by the WHH theory, which is determined by the $(dB_{c2}/dT)_{T=T_c}$ value (0.936 T/K for $B \perp ab$ and 1.615 T/K for $B \parallel ab$). In (b), the onset temperatures of the specific-heat transitions in various magnetic fields measured in the same sample (see [20]) are also shown for comparison.

set temperatures of the specific-heat transitions in $B \perp ab$ determined for the same sample (see Fig. S5(a) of the Supplemental Material [20]) is also shown. Extrapolations of the 50% ρ_N data in Figs. 4(b) and 4(d) give $B_{c2\perp} = 2.6$ T and $B_{c2\parallel} = 4.3$ T at 0 K, yielding the coherence lengths $\xi_{ab} = 11.3$ nm and $\xi_{c^*} = 6.8$ nm. The relatively small anisotropy in B_{c2} may seem strange for a superconductor with a quasi-2D Fermi surface, but a similar situation has been found in BaFe₂As₂-based superconductors [26, 27] and is believed to be due to a finite k_z dispersion of the cylindrical Fermi surface.

The $B_{c2}(T)$ behavior expected for a conventional superconductor from the Werthamer-Helfand-Hohenberg (WHH) theory [28] tends to saturate for $T \rightarrow 0$, as shown with solid lines in Figs. 4(b) and 4(d). On the other hand, our experimental data present much weaker tendency toward saturation. We note that the Pauli paramagnetic limit [28], $B_{\text{Pauli}} = 1.84 T_c = 5.3$ T, is larger than our B_{c2} , so the violation of the conventional behavior is not as strong as in the case of exotic superconductors like

UBe₁₃ [25]. Nevertheless, similar violations of the WHH theory as is found here have been discussed to be indicative of unconventional superconductivity in Cu_xBi₂Se₃ [13] and in Bi₂Se₃ under high pressure [14].

We have further characterized the CPSBS superconductor by measuring the lower critical field B_{c1} , which was determined to be 0.34 mT for $B \parallel ab$ at 0 K (Fig. S6(c) of the Supplemental Material [20]). Knowing $B_{c1\parallel}$, $B_{c2\perp}$, and $B_{c2\parallel}$, one can obtain the Ginzburg-Landau parameter $\kappa_{ab} = 192$, the penetration depths $\lambda_{ab} = 1.3$ μm and $\lambda_{c^*} = 2.2$ μm , and the thermodynamic critical field $B_c = 16.6$ mT [20]. The long penetration depths are consistent with the low carrier density and moderate disorder in CPSBS.

It is striking that all the bulk properties of the new superconductor CPSBS shown here point to possible occurrence of unconventional superconductivity accompanied with line nodes. The existence of line nodes implies a sign-changing gap function, which generically gives rise to surface Andreev bound states [29]. Strong spin-orbit coupling causes such surface Andreev states to be spin-split and form spin-non-degenerate Kramers pairs, which means that they become helical Majorana fermions [9]. Indeed, nodal superconductors with strong spin-orbit coupling have been discussed to be topological [11, 30]. Therefore, the superconductivity in CPSBS has a good chance to be topological and harbour Majorana fermions. To nail down the topological nature, making a Josephson junction with a conventional superconductor to measure a nontrivial current-phase relationship coming from boundary Majorana fermions [7, 8] would be a smoking-gun experiment.

We thank T. Toba for his help in synthesizing the samples, K. Eto and M. Kriener for technical assistance, and L. Fu, Y. Tanaka, A. Taskin, and A. Yamakage for helpful discussions. This work was supported by JSPS (KAKENHI 24740237, 24540320, and 25220708), MEXT (Innovative Area “Topological Quantum Phenomena” KAKENHI), AFOSR (AOARD 124038), and Inamori Foundation.

* Electronic address: y'ando@sanken.osaka-u.ac.jp

- [1] X.-L. Qi and S.-C. Zhang, Rev. Mod. Phys. **83**, 1057 (2011).
- [2] M. Z. Hasan and C. L. Kane, Rev. Mod. Phys. **82**, 3045 (2010).
- [3] Y. Ando, J. Phys. Soc. Jpn. **82**, 102001 (2013).
- [4] A. P. Schnyder, S. Ryu, A. Furusaki, and A. W. W. Ludwig, Phys. Rev. B **78**, 195125 (2008).
- [5] Y. Tanaka, M. Sato, and N. Nagaosa, J. Phys. Soc. Jpn. **81**, 011013 (2012).
- [6] Y. Maeno, S. Kittaka, T. Nomura, S. Yonezawa, K. Ishida, J. Phys. Soc. Jpn. **81**, 011009 (2012).
- [7] J. Alicea, Rep. Prog. Phys. **75**, 076501 (2012).

- [8] C. W. J. Beenakker, *Annu. Rev. Condens. Mat. Phys.* **4**, 113 (2013).
- [9] L. Fu and E. Berg, *Phys. Rev. Lett.* **105**, 097001 (2010).
- [10] Y. S. Hor, A. J. Williams, J. G. Checkelsky, P. Roushan, J. Seo, Q. Xu, H. W. Zandbergen, A. Yazdani, N. P. Ong, and R. J. Cava, *Phys. Rev. Lett.* **104**, 057001 (2010).
- [11] S. Sasaki, M. Kriener, K. Segawa, K. Yada, Y. Tanaka, M. Sato, and Y. Ando, *Phys. Rev. Lett.* **107**, 217001 (2011).
- [12] S. Sasaki, Z. Ren, A. A. Taskin, K. Segawa, L. Fu, and Y. Ando, *Phys. Rev. Lett.* **109**, 217004 (2012).
- [13] T. V. Bay, T. Naka, Y. K. Huang, H. Luigjes, M. S. Golden, A. de Visser, *Phys. Rev. Lett.* **108**, 057001 (2012).
- [14] K. Kirshenbaum, P. S. Syers, A. P. Hope, N. P. Butch, J. R. Jeffries, S. T. Weir, J. J. Hamlin, M. B. Maple, Y. K. Vohra, J. Paglione, *Phys. Rev. Lett.* **111**, 087001 (2013).
- [15] G. Goll, M. Marz, A. Hamann, T. Tomanic, K. Grube, T. Yoshino, and T. Takabatake, *Physica B* **403**, 1065 (2008).
- [16] N. P. Butch, P. Syers, K. Kirshenbaum, A. P. Hope, and J. Paglione, *Phys. Rev. B* **84**, 220504(R) (2011).
- [17] K. Nakayama, K. Eto, Y. Tanaka, T. Sato, S. Souma, T. Takahashi, K. Segawa, and Y. Ando, *Phys. Rev. Lett.* **109**, 236804 (2012).
- [18] L. Fang, C. C. Stoumpos, Y. Jia, A. Glatz, D. Y. Chung, H. Claus, U. Welp, W. K. Kwok, M. G. Kanatzidis, arXiv:1307.0260.
- [19] M. Kriener, K. Segawa, Z. Ren, S. Sasaki, and Y. Ando, *Phys. Rev. Lett.* **106**, 127004 (2011).
- [20] See Supplemental Material at [URL will be inserted by publisher] for materials and methods, supplemental data, and additional discussions.
- [21] M. Tinkham, *Introduction to Superconductivity* (McGraw-Hill, New York, 1975).
- [22] H. Won and K. Maki, *Phys. Rev. B* **49**, 1397 (1994).
- [23] K. Maki, *Superconductivity* (Ed. Parks, R. D., Marcel Dekker, New York, 1969).
- [24] G. E. Volovik, *JETP Lett.* **58**, 469 (1993).
- [25] M. B. Maple, J. W. Chen, S. E. Lambert, Z. Fisk, J. L. Smith, H. R. Ott, J. S. Brooks, M. J. Naughton, *Phys. Rev. Lett.* **54**, 477 (1985).
- [26] H. Q. Yuan, J. Singleton, F. F. Balakirev, S. A. Baily, G. F. Chen, J. L. Luo, N.L. Wang, *Nature* **457**, 565 (2009).
- [27] M. A. Tanatar, N. Ni, C. Martin, R. T. Gordon, H. Kim, V. G. Kogan, G. D. Samolyuk, S. L. Bud'ko, P. C. Canfield, R. Prozorov, *Phys. Rev. B* **79**, 094507 (2009).
- [28] N. R. Werthamer, E. Helfand, P. C. Hohenberg, *Phys. Rev* **147**, 295 (1966).
- [29] S. Kashiwaya and Y. Tanaka, *Rep. Prog. Phys.* **63**, 1641 (2000).
- [30] M. Sato and S. Fujimoto, *Phys. Rev. Lett.* **105**, 217001 (2010).

Supplemental Material

Materials and methods

High-quality single crystals of $(\text{PbSe})_5(\text{Bi}_2\text{Se}_3)_6$ (PSBS) were grown by a modified Bridgman method using high purity elements Pb (99.998%), Bi (99.9999%), and Se (99.999%) with the starting composition of Pb:Bi:Se = 7:26:46 in a sealed evacuated quartz tube at 698 °C for 6 h, followed by a slow cooling to 650 °C with a cooling rate of 12 °C/day and then quenching to room temperature. The phase diagram of the Pb-Bi-Se ternary system is very complicated [31], which causes multiple crystal phases to coexist in a boule. After the growth, we chose the PSBS phase based on the x-ray diffraction analysis of the crystals cut out from the boule [15]. Roughly 30% of a boule is in the $m = 2$ PSBS phase. For the electrochemical Cu intercalation, we used a saturated solution of CuI powder (99.99%) in acetonitrile CH_3CN [32]. Samples with a typical size of $2 \times 1 \times 0.2 \text{ mm}^3$ were wound by a 50- μm thick, bare Cu wire, and they together acted as the working electrode. A 0.5-mm thick Cu stick was used as both the counter and reference electrode. The concentration of intercalated Cu was determined from the weight change before and after the intercalation process, giving the x value of $\text{Cu}_x(\text{PbSe})_5(\text{Bi}_2\text{Se}_3)_6$ (CPSBS). The samples were then annealed in a sealed evacuated quartz tube at 550 °C for 2 h and quenched by dropping the quartz tube into cold water to activate the superconductivity.

The dc magnetic susceptibility was measured with a commercial SQUID magnetometer (Quantum Design MPMS-1); the remnant field was removed with the magnet reset procedure and the error in the applied field was less than 0.01 mT. The resistivity ρ_{xx} and the Hall resistivity ρ_{yx} were measured by using a standard six-probe method where the contacts were made by attaching gold wires with a vacuum-cure silver paint. The Hall coefficient R_H was calculated from the slope of $\rho_{yx}(B)$. The specific heat c_p was measured with a relaxation-time method using a commercial equipment (Quantum Design PPMS-9). To confirm the reproducibility of the specific-heat data, we made detailed measurements on two superconducting samples with nearly 100% shielding fractions, $x = 1.36$ and 1.66, both of which had $T_c = 2.85 \text{ K}$.

S1. Carrier density and Cu intercalation

Temperature dependencies of R_H in pristine PSBS and superconducting CPSBS ($x = 1.36$) are shown in Fig. S1(a). The carrier density n_e is calculated from the value of R_H at 4 K, and it is $4 \times 10^{20} \text{ cm}^{-3}$ in PSBS and $1.2 \times 10^{21} \text{ cm}^{-3}$ in CPSBS. The magnetic-field dependence of ρ_{yx} in CPSBS at 4 K is essentially linear, indicating that only one type of electron carriers dominate the transport properties; namely, the physics is dominated by only one band. This suggests that the topological and nontopological bands of the Bi_2Se_3 unit observed in PSBS [15] may well have merged at the chemical potential of CPSBS that has been raised due to the electron doping.

In CPSBS samples, the volume density of Cu atoms is given by $n_{\text{Cu}} = x(d/M)N_A$, where $d = 7.715 \text{ g/cm}^3$ is the density of PSBS, $M = 5359.8 \text{ g/mol}$ is the molar mass, and N_A is the Avogadro constant. For $x = 1.36$, one obtains $n_{\text{Cu}} = 1.18 \times 10^{21} \text{ cm}^{-3}$. On the other hand, the increase in the electron carrier density upon Cu intercalation in this sample is given by $\Delta n_e = (1.2 \times 10^{21}) - (4 \times 10^{20}) = 8 \times 10^{20} \text{ cm}^{-3}$. Therefore, one can estimate that each intercalated Cu introduces $\Delta n_e/n_{\text{Cu}} = 0.68$ electron on average, which is much more efficient than in $\text{Cu}_x\text{Bi}_2\text{Se}_3$ [10].

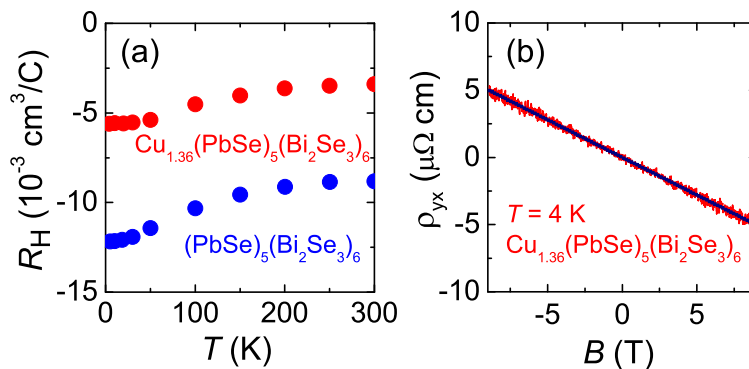


FIG. S1: (a) Temperature dependencies of the Hall coefficient R_H in pristine PSBS and superconducting CPSBS ($x = 1.36$). (b) Magnetic-field dependence of ρ_{yx} measured in CPSBS ($x = 1.36$) at 4 K. The solid line emphasizes the linear nature of the B dependence.

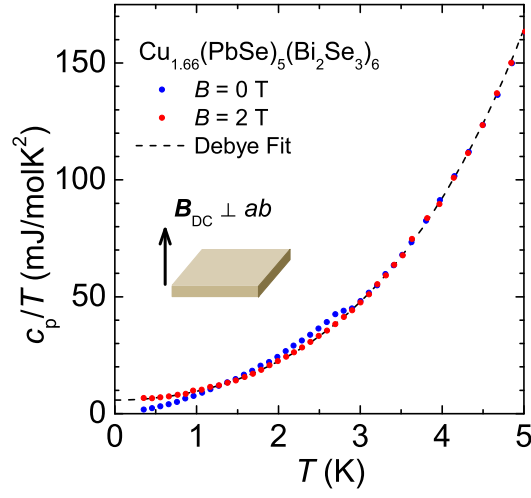


FIG. S2: c_p/T vs T data measured in 0 and 2 T applied perpendicular to the ab plane. The dashed line is the Debye fitting to the 2-T data.

S2. Specific heat analyses

The temperature dependence of the total specific heat c_p , which includes both the phononic and electronic contributions, c_{ph} and c_{el} , respectively, is shown in Fig. S2 for 0 and 2 T. The conventional Debye fitting using

$$c_p = c_{el} + c_{ph} = \gamma_N T + A_3 T^3 + A_5 T^5 \quad (1)$$

to the 2 T data, which represent mostly the normal-state behavior in the fitted temperature range, describes well the data up to 5 K. From this fitting we obtain the normal-state electronic specific-heat coefficient $\gamma_N = 5.89$ mJ/mol K². Assuming that the system is quasi-2D, this γ_N corresponds to the effective mass $m^* = (3\hbar^2 c^* \gamma_N) / (V_{mol} k_B^2) = 2.6m_e$, where $c^* = 5.06$ nm is the lattice constant along the c^* direction, $V_{mol} = 694.7$ cm³/mol is the molar volume, and

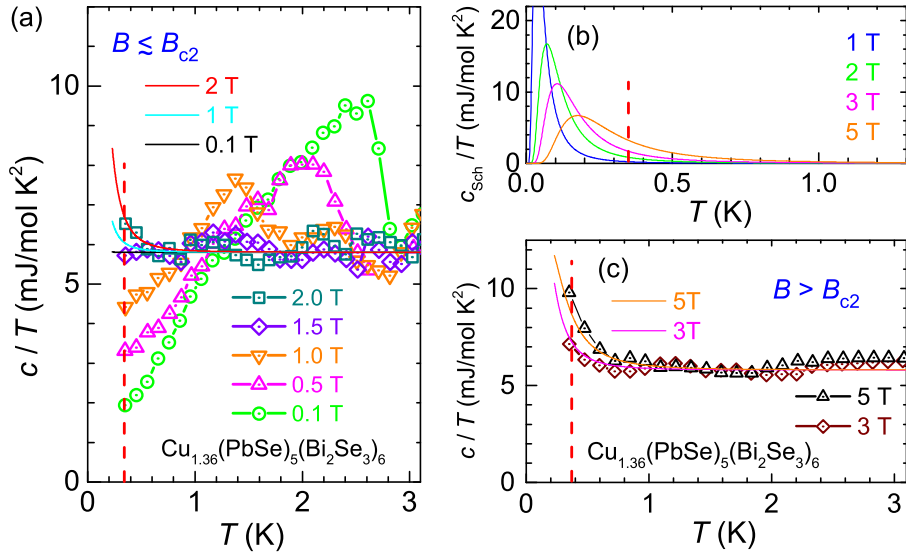


FIG. S3: Schottky anomaly in the $x = 1.36$ sample. (a) $(c_p - c_{ph})/T$ vs T data for $B \lesssim B_{c2}$ (symbols), together with the calculated $c_{Sch}/T + \gamma_N$ for $B = 0.1, 1,$ and 2 T (solid lines). (b) Theoretical curves of the expected Schottky contribution c_{Sch}/T coming from 0.037% of $S = 1/2$ moments with the Landé g factor of 0.17. Those parameters are determined to consistently reproduce the data for the $x = 1.36$ sample in 2 – 5 T. (c) $(c_p - c_{ph})/T$ vs T data for $B > B_{c2}$ and the calculated $c_{Sch}/T + \gamma_N$ for $B = 3$ and 5 T (solid lines). In panels (a)-(c), vertical red dashed lines mark the lowest experimental temperature.

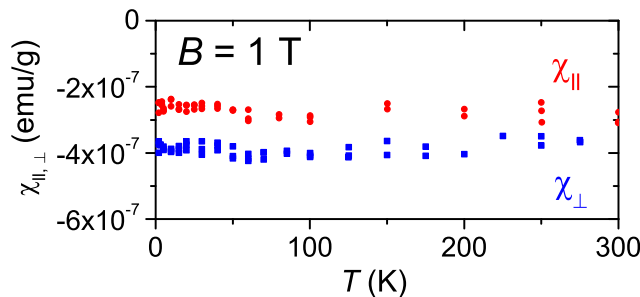


FIG. S4: Normal-state magnetic susceptibilities χ_{\perp} and χ_{\parallel} measured on the $x = 1.66$ sample down to 1.8 K in 1 T applied perpendicular and parallel to the ab plane, respectively.

m_e is the free electron mass. The coefficients of the phononic contribution are $A_3 = 3.73$ mJ/mol K⁴ and $A_5 = 0.10$ mJ/mol K⁶, and the former gives the Debye temperature $\theta_D = 153.1$ K.

We found that in high magnetic fields (above ~ 1.5 T), a Schottky anomaly becomes noticeable in the $c_p(T)$ data at low temperature. We therefore analyzed the small Schottky contribution $c_{\text{Sch}} \equiv c_p - c_{\text{ph}} - c_{\text{el}}$ using the two-level Schottky model with free $S = 1/2$ moments [33, 34],

$$c_{\text{Sch}}(T, B) = \frac{nx^2 e^x}{(1 + e^x)^2} \quad \left(x \equiv \frac{g\mu_B B}{k_B T} \right), \quad (2)$$

where g is the Landé g factor and n is a coefficient in the unit of the universal gas constant R . The temperature below which an upturn starts is determined solely by the g factor, which is found to be 0.17 from the data of the $x = 1.36$ sample in high magnetic fields above B_{c2} [Fig. S3(c)]; such a small g factor has been reported to come from an anisotropy caused by crystal fields [35–38] or from hyperfine-enhanced nuclear magnetic moments [39, 40]. The upturns in the 2 – 5 T data shown in Figs. S3(a) and S3(c) are consistently reproduced by Eq. (2) with the coefficient $n = 3.1$ mJ/mol K, which corresponds to the free-moment concentration of only $\sim 0.037\%$. It is worth emphasizing that the superconductivity in CPSBS is already suppressed above ~ 2 T at 0.35 K, so the observed Schottky anomaly is largely irrelevant when one discusses the specific-heat behavior in the superconducting state. The calculated curves in Fig. S3(b) show that the peak due to this Schottky anomaly is expected to occur at a much lower temperature than our experimental range.

To gain insight into the origin of this small Schottky anomaly, we have measured the normal-state magnetic susceptibilities χ_{\perp} and χ_{\parallel} for $B \perp ab$ and $B \parallel ab$, respectively, down to the lowest temperature of our SQUID magnetometer, 1.8 K. The result is shown in Fig. S4, where one can see that there is no visible Curie behavior in neither of the field directions. If the Schottky anomaly was due to $\sim 0.037\%$ of $S = 1/2$ free electron spins that happen to have a small g factor for $B \perp ab$ due to crystal fields, they should give rise to a visible Curie behavior for $B \parallel ab$ above 1.8 K, but we did not observe it. Therefore, one may conclude that the observed small Schottky anomaly is likely to be due to hyperfine-enhanced nuclear magnetic moments, which originate from a minority valence state or a minority isotope of the constituent elements of CPSBS, or from some impurities that may have entered into the samples during the Cu intercalation process. However, it is difficult to name the actual element/isotope, because various nuclei can have hyperfine-enhanced moments and the concentration of the nucleus in question is only $\sim 0.037\%$. In any case, the determination of the exact source of the weak Schottky anomaly is not very important for the present study, as long as its contribution can be duly subtracted.

To make our best effort to quantify the magnetic-field dependence of c_{el} in the superconducting state, we calculated $c_{\text{Sch}}(T, B)$ (which is only $\lesssim 20\%$ of c_{el} at 0.35 K in 2 T and is negligible in 1 T) and subtracted it from all the specific-heat data in magnetic fields. The c_{el}/T vs T data measured in the $x = 1.36$ sample in various magnetic fields applied perpendicular to the ab plane are shown in Fig. S5(a) after the subtraction of $c_{\text{Sch}}(T, B)/T$; for comparison, Fig. S3(a) shows the data for $(c_p - c_{\text{ph}})/T$ before subtraction of c_{Sch}/T , as well as the calculated Schottky component in terms of $c_{\text{Sch}}(T, B)/T + \gamma_N$ for selected field values. The $c_{\text{el}}(B)$ behavior at 0.35 K for this sample is shown in Fig. S5(b), which is best described with $c_{\text{el}} \sim B^{0.56}$; in this figure, we also show the uncorrected $c_{\text{el}}(B)$ data including the Schottky contribution, the effect of which does not qualitatively change the behavior. The power 0.56 obtained for $c_{\text{el}}(B)$ is consistent with the result for the $x = 1.66$ sample shown in the main text [Fig. 3(b)]. The parameters of the Schottky contribution used for obtaining the c_{el}/T data for the $x = 1.66$ sample shown in Fig. 3(a) of the main text were the same as those for the $x = 1.36$ sample.

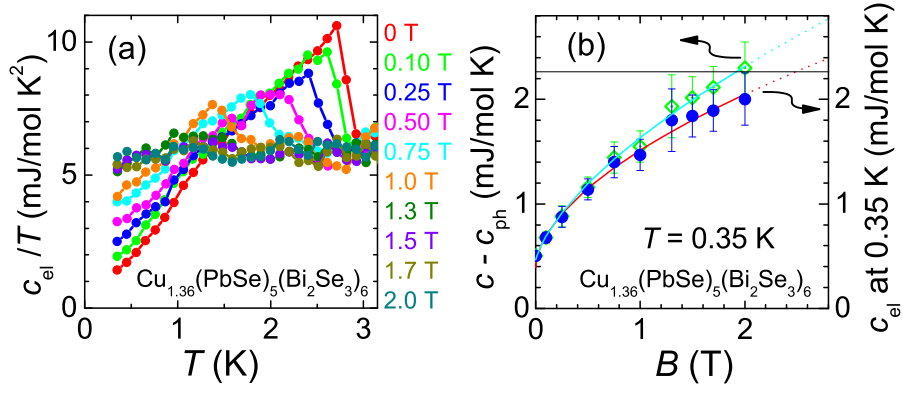


FIG. S5: (a) c_{el}/T vs T plots for various magnetic fields ($B \perp ab$) after subtracting the small Schottky contribution in CPSBS ($x = 1.36$). (b) Magnetic-field dependence of c_{el} at 0.35 K taken from the data shown in (a). The red solid line is the best fit of the function $aB^n + c_0$ to the data and gives $n = 0.56 \pm 0.06$, $a = 1.12 \pm 0.06 \text{ mJ mol}^{-1} \text{ K}^{-1} \text{ T}^{-n}$, and $c_0 = 0.39 \pm 0.05 \text{ mJ mol}^{-1} \text{ K}^{-1}$. For comparison, we also show with light-green diamonds the B dependence of $c - c_{ph}$ at 0.35 K without subtracting the Schottky contribution; the light-blue solid line is the best fit of the same function, yielding $n = 0.63 \pm 0.06$, $a = 1.3 \pm 0.1 \text{ mJ mol}^{-1} \text{ K}^{-1} \text{ T}^{-n}$, and $c_0 = 0.4 \pm 0.5 \text{ mJ mol}^{-1} \text{ K}^{-1}$. Horizontal solid line corresponds to $\gamma_N T$ at $T = 0.35$ K.

As one can see in Fig. S5(a), the c_{el}/T vs T behavior broadens significantly in high magnetic fields above ~ 1 T, which makes it impossible to determine the mid-point of the specific-heat jump. We therefore try to extract the information about B_{c2} from c_{el}/T by determining, with a certain error bar, the onset temperature below which c_{el}/T deviates from γ_N , and such data are plotted in Fig. 4(b) of the main text.

S3. Superconducting parameters

Figure S6 summarizes the results of the magnetization measurements of the $x = 1.66$ sample to determine the lower critical field B_{c1} . Figure S6(a) shows $M(B)$ curves measured after zero-field cooling to various temperatures in magnetic field applied parallel to the ab plane. We define B_1 at each temperature as the value at which the $M(B)$ data deviates from its initial linear behavior, as can be seen in Fig. S6(b). To obtain $B_{c1\parallel}$, those B_1 values are corrected for the demagnetization effect, though it is small for $B \parallel ab$: Using the approximation given for the slab geometry [41], we obtain $B_{c1\parallel} = B_1 / \tanh \sqrt{0.36b/a}$, with the aspect ratio $b/a = 1.6/0.23$ in the present case. The resulting $B_{c1\parallel}$ values are shown in Fig. S6(c). To determine the 0-K limit, we used the empirical formula $B_{c1}(T) = B_{c1}(0)[1 - (T/T_c)^4]$ [42] and obtained $B_{c1\parallel}(0) = 0.34$ mT. Note that the flux pinning in the present system is weak as evidenced by the small magnetic hysteresis [Fig. S7], which supports the reliability of the determination of B_{c1} using the above method [19].

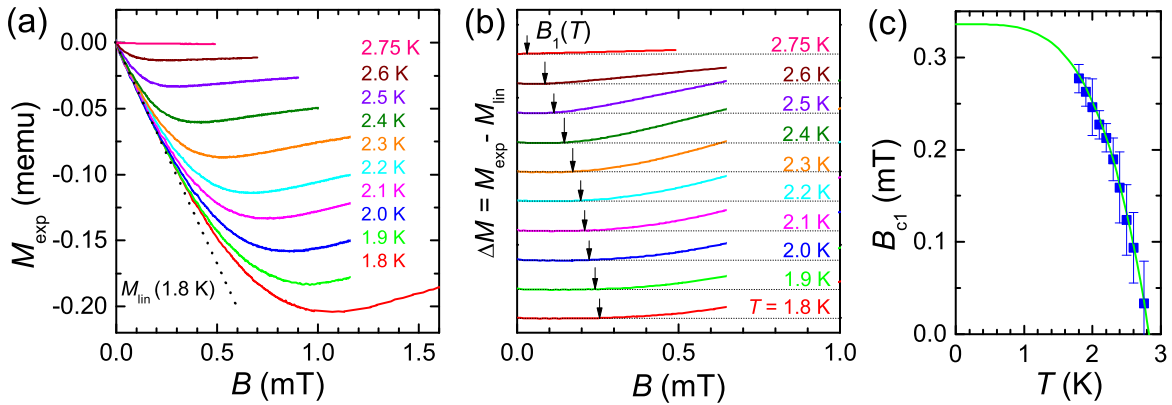


FIG. S6: (a) Initial $M(B)$ behavior of the $x = 1.66$ sample after zero-field cooling to various temperatures. (b) Plots of $\Delta M \equiv M - aB$, where a is the initial slope, together with the determination of B_1 shown by arrows. (c) $B_{c1\parallel}$ vs. T phase diagram; the solid line is a fit to the empirical formula shown in the text.

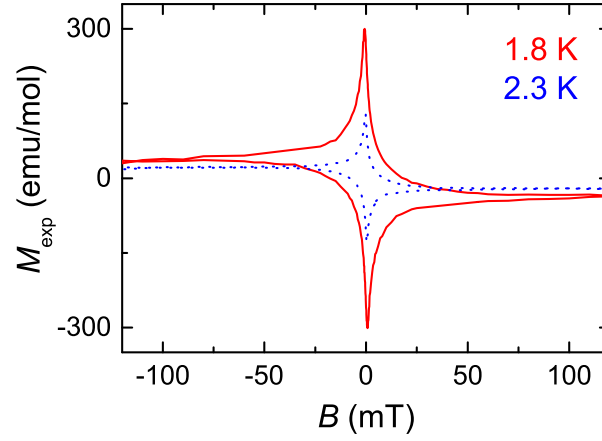


FIG. S7: $M(B)$ curves measured on the $x = 1.66$ sample at 1.8 and 2.3 K after subtracting the diamagnetic background.

From $B_{c2\perp} = 2.6$ T, the coherence length $\xi_{ab} = \sqrt{\Phi_0/(2\pi B_{c2\perp})} = 11.3$ nm is obtained, while from $B_{c2\parallel} = 4.3$ T, we use $\xi_{ab}\xi_{c^*} = \Phi_0/(2\pi B_{c2\parallel})$ and obtain $\xi_{c^*} = 6.8$ nm. The anisotropy ratio is calculated as $\gamma = B_{c2\parallel}/B_{c2\perp} = \lambda_{c^*}/\lambda_{ab} = 1.65$; here, λ_{c^*} and λ_{ab} are the penetration depths along the c^* and ab directions, respectively. Since we have the B_{c1} value only for $B\parallel ab$, we define the effective GL parameter $\kappa_{ab} \equiv \sqrt{\lambda_{ab}\lambda_{c^*}/\xi_{ab}\xi_{c^*}}$ and use $B_{c1\parallel} = \Phi_0 \ln \kappa_{ab}/(4\pi\lambda_{ab}\lambda_{c^*})$ together with $B_{c2\parallel}/B_{c1\parallel} = 2\kappa_{ab}^2/(\ln \kappa_{ab} + 0.5)$ [43, 44] to obtain $\kappa_{ab} \approx 192$. We then obtain the thermodynamic critical field $B_c = \sqrt{B_{c1\parallel}B_{c2\parallel}/\ln \kappa_{ab}} = 16.6$ mT and the penetration depths $\lambda_{ab} = \kappa_{ab}\sqrt{\xi_{ab}\xi_{c^*}/\gamma} = 1.3$ μm and $\lambda_{c^*} = 2.2$ μm .

* Electronic address: y'ando@sanken.osaka-u.ac.jp

- [10] Y. S. Hor *et al.*, Phys. Rev. Lett. **104**, 057001 (2010).
- [15] K. Nakayama, K. Eto, Y. Tanaka, T. Sato, S. Souma, T. Takahashi, K. Segawa, and Y. Ando, Phys. Rev. Lett. **109**, 236804 (2012).
- [19] M. Kriener, K. Segawa, Z. Ren, S. Sasaki, and Y. Ando, Phys. Rev. Lett. **106**, 127004 (2011).
- [31] L. E. Shelimova, O. G. Karpinskii, V. S. Zemskov, Inorg. Mater. (USSR) **44**, 927 (2008).
- [32] M. Kriener, K. Segawa, Z. Ren, S. Sasaki, S. Wada, S. Kuwabata, and Y. Ando, Phys. Rev. B **84**, 054513 (2011).
- [33] J. P. Emerson, R. A. Fisher, N. E. Phillips, D. A. Wright, E. M. McCarron III, Phys. Rev. B **49**, R9256 (1994).
- [34] K. A. Moler *et al.*, Phys. Rev. B **55**, 3954 (1997).
- [35] S. Holmes, D. K. Maude, M. L. Williams, J. J. Harris, J. C. Portal, K. W. J. Barnham, C. T. Foxon, Semicond. Sci. Technol. **9**, 1549 (1994).
- [36] R. M. Hannak, M. Oestreich, A. P. Heberle, W.W. Rühle, K. Köhler, Solid State Comm. **93**, 313 (1995).
- [37] P. Le Jeune, D. Robart, X. Marie, T. Amand, M. Brousseau, J. Barrau, V. Kalevich, D. Rodichev, Semicond. Sci. Technol. **12**, 380 (1997).
- [38] H. P. van der Meulen *et al.*, Physica C **152**, 65 (1988).
- [39] K. Andres, E. Bucher, J. Appl. Phys. **42**, 1522 (1971).
- [40] R. Movshovich, M. Jaime, J. D. Thompson, C. Petrovic, Z. Fisk, P. G. Pagliuso, J. L. Sarrao, Phys. Rev. Lett. **86**, 5152 (2001).
- [41] E. H. Brandt, Phys. Rev. B **60**, 11939 (1999).
- [42] M. Kriener, K. Segawa, S. Sasaki, and Y. Ando Phys. Rev. B **86**, 180505(R) (2012).
- [43] Clem, J. R. Phenomenological theory of magnetic structure in the high-temperature superconductors. Physica C **162-164**, 1137-1142 (1989).
- [44] Hu, C.-R. Numerical constants for isolated vortices in superconductors. Phys. Rev. B **6**, 1756-1760 (1972).